JBC Papers in Press. Published on July 20, 2018 as Manuscript RA118.004043
The latest version is at http://www.jbc.org/cgi/doi/10.1074/jbc.RA118.004043

The rational design of affinity attenuated OmCI for the purification of Complement C5

Alex Macpherson[1,2]*, Xiaofeng Liu[1], Neesha Dedi[1], Jeffery Kennedy[1], Bruce Carrington[1], Oliver Durrant[1], Sam Heywood[1], Jean van den Elsen[2] and Alastair D.G. Lawson[1]

Running title: *The rational design of affinity attenuated OmCI*

From [1]UCB-Celltech, 216 Bath Road, Slough, UK. SL1 3WE; [2] Department of Biology and Biochemistry, University of Bath, Bath, UK. BA2 7AX.

*To whom correspondence should be addressed: Alex Macpherson, UCB-Celltech, 216 Bath Road, Slough, UK. SL1 3WE. Email: Alex.Macpherson@ucb.com

Key words: complement system, mutagenesis, purification, biophysics, immune evasion, OmCI, complement component C5

Abstract

Complement component C5 is the target of the monoclonal antibody Eculizumab, and the focus of a sustained drug discovery effort to prevent complement-induced inflammation in a range of autoimmune diseases.

The immune evasion protein OmCI binds to, and potently inactivates, C5; this tight-binding interaction can be exploited to affinity-purify C5 protein from serum, offering a vastly simplified protocol compared to existing methods. However, breaking the high-affinity interaction requires conditions which risk denaturing or activating C5.

We performed structure-guided in silico mutagenesis to identify prospective OmCI residues that contribute significantly to the binding affinity. We tested our predictions in vitro, using site directed mutagenesis, and characterised mutants using a range of biophysical techniques as well as functional assays. Our biophysical analyses suggest the C5-OmCI interaction is complex with potential for multiple binding modes.

We present single mutations that lower the affinity of OmCI for C5 and combinations of mutations that significantly decrease, or entirely abrogate, formation of the complex. The affinity attenuated forms of OmCI are suitable for affinity purification and allow elution under mild conditions that are non-denaturing or activating to C5.

We present the rational design, biophysical characterisation and experimental validation of affinity reduced forms of OmCI as tool reagents to enable the affinity purification of C5.

Complement component C5 is a large, 188 kDa protein which is integral to the complement system. As an eventual consequence of activation of any of the classical, lectin or alternative pathways, C5 is cleaved into two functionally distinct moieties (1,2). The smaller anaphylatoxin subunit C5a signals via C5aR, a pro-inflammatory G-Protein Coupled Receptor (3,4). The cleavage of C5a triggers a major conformational change in the C5d-CUB-MG8 superdomain, forming the metastable C5b subunit (5). The conformationally primed C5b can then assemble with C6-C9 to form the membrane attack complex, which results in the targeted lysis of pathogenic or damaged cells (6-8).

Complement C5 has been targeted with various therapeutics, most notably by Eculizumab, a monoclonal antibody that binds to the MG7 domain of C5 (9,10) preventing cleavage by both the alternative pathway C5 convertase (C3bBbC3b) or the classical and lectin pathways' convertase (C4bC2aC3b) (1,2,10-12). Eculizumab is approved for the treatment of paroxysmal nocturnal haemoglobinuria (PNH) (13,14) and atypical haemolytic uraemic syndrome (aHUS) (15,16), and clinical studies are underway to expand into indications including age-related macular degeneration (17,18), myasthenia gravis (19,20), optic neuritis (21), and kidney

transplant rejection (22,23). Second generation therapeutics including affibodies, cyclic peptides, aptamers and small molecules that target C5 are currently in clinical or pre-clinical development (24,25).

Intriguingly, parasites have also developed strategies of targeting C5 to evade lysis by the complement system. Two species of tick, *Ornithodoros moubata* and *Rhipicephalus appendiculatus*, have independently evolved salivary proteins that inactivate C5 when secreted during feeding (9,26-29). The two proteins, dubbed OmCI and RaCI after their respective species of origin, are of comparatively low molecular weight and are distinct in both sequence and structure.

A crystal structure of the C5:OmCI:RaCI ternary complex (9) shows that both proteins bind at opposing ends of the C5d domain of C5, anchoring it to neighbouring domains. These sites are distant from the Eculizumab and Cobra Venom Factor binding sites on the MG7 domain (10,30), and may prevent C5 activation by a different inhibitory mechanism.

OmCI, a 17 KDa protein exhibiting the eight-stranded, antiparallel β-barrel fold characteristic of the lipocalin family, binds with the C5d and CUB domains of C5 (9,26). While it does not appear to have bonded interactions with the neighbouring, highly mobile C345C domain, such is their proximity that OmCI may still influence its conformational sampling.

As a lipocalin, OmCI has evolved to interact with small hydrophobic molecules (31). In addition to preventing release of C5a, OmCI also sequesters the proinflammatory molecule leukotriene B4 (LTB4), making it a potent inhibitor of the early inflammatory response (27). A crystal structure of the OmCI/LTB4 complex shows the aliphatic chain of LTB4 bound within a conical binding cavity in the centre of the β-barrel fold (28). The pocket is comparatively promiscuous, also binding palmitoleic and elaidic fatty acids. OmCI can bind LTB4 and C5 simultaneously in a non-cooperative manner (28).

OmCI has broad cross-species reactivity and is being developed commercially in a modified form as Coversin (32), primarily targeting patients with the R885H mutation – a perturbation to the Eculizumab epitope which renders them resistant to treatment with the monoclonal antibody (33,34).

Akin to C3 and C4, C5 is comparatively abundant in serum at a concentration of 75 ug/mL (35). It expresses poorly in recombinant systems and is usually purified from serum. The standard protocol involves a serum precipitation step, followed by two sequential ion exchange purifications and a gel filtration step (36,37). Alternative purification approaches have been described, including hydrophobic interaction chromatography and immunoadsorption (38,39). Immunoadsorption is incumbent on the immunisation of animals to generate a polysera which, unless a monoclonal antibody is used, may not be a specific capture mechanism, with only a proportion of the sera being specific to C5 and with the potential for inconsistent performance due to batch variation. An additional complication is that changes in pH have been shown to activate C5 and subsequently mild, non-activating elution conditions must be found to break the interaction with the antibody (37).

The C5-OmCI interaction has been previously exploited to purify C5 and OmCI complexes for crystallography (9). OmCI expresses extremely well in bacterial, yeast or mammalian cells, with a yield of 0.4g/L reported in yeast (28). It binds C5 with high affinity and, with suitable modifications to modulate affinity, could be an ideal recombinant tool with which to purify C5 from serum.

The crystal structure allows computational energy calculations to guide the selection of residues to be attenuated using mutations to alanine or glycine. These rationally designed mutants may display differing affinities but also changing susceptibility to pH or ionic conditions, which may be exploited to create a specific recombinant reagent for affinity purification. If discovered, these reagents would markedly simplify the purification of complement C5 and aid academic and industrial research.

Results

In silico design of affinity impaired OmCI mutants

Using information from the crystal structure of the C5-OmCI-RaCI complex, we designed single residue mutations to reduce OmCI-C5 affinity using Molecular Operating Environment (MOE) software (40,41) (Figure 1). Mutations were ranked by the dAffinity score, a surrogate for binding free energy. Mutations predicted to lower the energy of the interaction more than 1 kcal/mol were found (Table 1).

Notably, our analysis has selected charged residues that appear to participate in salt bridges or hydrogen bonds. Two hydrophobic residues, M134 and L140, were also identified. When mutating hydrophobic residues, we chose glycine mutations rather than alanine, to make a non-clashing mutation where hydrophobicity was entirely absent from the side chain.

Validation of affinity impaired OmCI mutants

To test our predictions, we made the following single residue mutations: R47A, H117A, M134G, L140G, E141A, H164A and D167A. In addition, a control F36W mutation was made. This mutation is patented as abrogating LTB4 binding without altering the affinity for C5 (42). We tested these OmCI mutants by SPR in single cycle kinetics experiments, with the aim of identifying a smaller panel of mutants to profile as a purification reagent. Single-cycle kinetics is performed by sequentially injecting increasing concentrations of analyte over the sensor chip, in the absence of any regeneration steps to remove bound analyte from the previous injection.

The sensorgrams could be fitted using a single site binding model but were better explained by including additional parameters in a heterogenous ligand model. When using the single site binding model, comparatively low standard errors (SE), <0.2%, were observed when fitting the rate constants. However, visually, the model appeared to poorly estimate the on-rate (k_{on}), overestimating the k_{on} at lower concentrations and underestimating at higher concentrations (Figure S1).

Accordingly, we opted to rank the mutations based on changes in off-rate (k_{off}), which was paramount for affinity purification (Table 1). Two mutations, E141A and M134G, had a significant effect on the stability of the OmCI-C5 complex. The E141A mutation increased the k_{off} value of the complex by ~29x and the M134G mutation by ~229x. However, we were concerned that the M134G mutant displayed low binding, relative to the amount of immobilised material, suggesting the protein had either been expressed with low activity or partially inactivated through amine coupling to the sensor chip. Other mutations had only modest effects on k_{off}. The control F36W mutation, which is distal to the interface with C5, showed a small increase in k_{off} value and displayed the same stoichiometric ratio of binding as wt OmCI.

Our sensorgrams suggest that the OmCI-C5 interaction is complex, and we chose to investigate further in multi-cycle kinetics experiments which are described later.

Designing a suitable C5 purification reagent ligand based on combined OmCI mutations

In order to further lower affinity, we modelled combinations of mutations. Again, we used MOE to simulate changes in binding energy (Table 1). Due to the potential for synergy, we retained mutations that had previously shown little effect in this second round of designs and based our final selection on the output of our MOE analysis.

As predicted, combining mutations further abridge and, in some cases, entirely abrogate binding to C5. Combining either the H164A or R47A mutations with E141A produced OmCI variants with k_{off} 197-973x faster than wt OmCI – characteristics favourable for application as affinity purification reagents, retaining fast association with C5, but with markedly increased dissociation.

The largest effect was observed in the E141A/ R47A/ H164A/ L140G quadruple mutant, which produced a square wave sensorgram, more characteristic of the fast binding kinetics of a low molecular weight chemical fragment than a protein-protein interaction. The k_{off} value of this protein was ~5,500x higher than wt OmCI. The M134G mutation completely prevented binding when used in combination with E141A and R47A.

Structural and functional analysis

Circular Dichroism

To look for gross changes in the secondary structure we used circular dichroism (CD). We

tested the E141A/ R47A and E141A/ H164A double mutants, alongside their constituent single mutants: E141A, R47A and H164A (Table 1). The M134G mutant, which markedly increased the k_{off} value but significantly lowered binding, was also tested. The CD traces were closely comparable with wt OmCI, except for M134G, which showed a marked loss of structure at 217 nm consistent with an increase in random coil. Loss of the positive peak at 190 nm was also observed, suggesting a loss of overall secondary structure (Figure S2).

Differential Scanning Calorimetry

We assessed the thermal stability of the mutants, their ability to refold after denaturation, and their capacity to stabilise C5 when complexed using Differential Scanning Calorimetry (DSC).

C5 displays a biphasic unfolding; the main peak unfolded at 60 ºC, displaying a shoulder at 69 °C, while a smaller, more stable domain or conformer unfolded at 77 ºC (Table 2 and Figure 2). Upon complexing with OmCI the main peak was stabilised significantly with a ΔTm +8.6 ºC. The mutants also increase the thermal stability of the main peak, with the degree of stabilisation reducing in agreement with their attenuated affinity.

The second peak may be stabilised upon OmCI binding, but the effect is smaller. The area under the peak, corresponding to the enthalpy of unfolding remains broadly the same, and the relationship to the affinity of the OmCI construct used is not as clear as observed with stabilisation of the main peak.

The OmCI mutants are themselves typically less thermally stable than wt OmCI (Table 1, Figure 2 and Table S1). The most destabilising OmCI mutation was M134G, followed by R47A and E141A. The remaining mutants had comparatively modest ΔTm of <-3 ºC. Of note, the E141A/ R47A double mutant was more thermally stable than wt OmCI, despite the single R47A and E141A mutations being amongst the most destabilising.

We performed a cycle of cooling prior to a second melt to assess the ability of the proteins to refold after denaturation. The peak area corresponds to the enthalpy of unfolding (ΔH) and by taking a ratio of the two peaks a ΔΔH or percentage of refolding can be calculated. As a large, complex protein with numerous disulphide bonds, C5 was unable to refold, but a proportion of OmCI could recover and be re-melted at a Tm almost identical to the first cycle. There was around a 72% recovery for wt OmCI with 47-69% recovery of the mutants. Consistent with the CD data, the M134G mutant was largely unable to refold with only 24% of protein recovered.

SPR - multi cycle kinetics

Due to our observations when fitting data in our single cycle kinetics experiments, we looked for further evidence of complex binding kinetics in the C5-OmCI interaction. In order to obtain more detailed kinetic data for our analysis, we performed multi-cycle kinetics experiments by SPR. Multi-cycle kinetics performs a single injection of a single sample concentration within a cycle, regenerating the surface after each injection to dissociate bound material. To exclude heterogeneity in the immobilisation steps, OmCI was uniformly immobilised in a fixed orientation, using biotin conjugated to an N-terminal AVI tag.

These data were explained by a single site binding model, with the fitting of k_{on} generating broadly acceptable SE values. The refractive index changes upon binding did not suggest that the binding stoichiometry exceeded 1:1. However, consistent with our single cycle experiments, the single site binding model again appeared to underestimate k_{on} at low concentrations and overestimate at higher concentrations (Figure 3). This suggests that observations in single cycle kinetics experiments were not the result of heterogenous immobilisation to the sensor chip and may indicate additional complexity in the OmCI-C5 binding interaction.

We report individual rate constants and K_D values for the mutant OmCI proteins binding to C5 (Table 1, Figure 3 and Table S2). The wt protein exhibited antibody-like affinity, exceeding the 1.0E-5 s^{-1} limit for accurate determination of k_{off} by SPR (43). In our experiments, the K_D of wt OmCI is <100 pM, at least ten-fold lower than previously reported (28). The E141A single mutant displayed a >7-fold decrease in affinity (K_D of 0.7 nM), and the E141A/H164A double mutant displayed a >40-fold decrease in affinity (K_D of 4 nM). Finally, the E141A/R47A double mutant displayed a >130-fold decrease in affinity (K_D of 13 nM), relative to wt. Importantly, these decreases in

affinity were mediated by increases in the k_{off} values.

Complement Activation ELISA

We tested the mutants in an Alternative Pathway (AP) activation ELISA to establish the extent to which affinity abridged forms of OmCI could inhibit formation of the MAC (Table 1, Table S3 and Figure S3). The single mutants and wt OmCI were potent inhibitors, displaying steep Hill slopes indicating that they had reached the tight binding limit of the assay. The double mutants, E141/ R47A and E141A/ H164A, showed a >10-fold and >5-fold loss of potency, respectively. Despite the variation in potency, all the mutants could effectively inhibit formation of the MAC at sufficiently high concentrations.

Affinity purification of C5 with the E141A, H164A double mutant

Having engineered faster dissociating forms of OmCI, we began to develop methods for the affinity purification of C5 from serum. OmCI proteins were biotinylated via an N-terminal tag and captured on a streptavidin column. Fractionated serum was applied to the column and conditions for the elution of C5 were tested.

With wt OmCI (k_{off} =<1.0E-5 s^{-1}), C5 was captured but would not elute with either 2M NaCl or 3M $MgCl_2$. Using a pH gradient, C5 was eluted at approximately pH 2.8, where it formed a milky precipitate which could be reversed upon neutralisation with 1M Tris.

Working to the 'Goldilocks principle', we hoped to identify a mutant with the ideal kinetic profile to permit capture of C5 but with a suitably attenuated k_{off} to allow the interaction to be destabilised and eluted under mild conditions.

We ran small scale purifications, trialling the mutants as capture reagents in order of their faster dissociation. The E141A single mutant (k_{off} =3.0E-04 s^{-1}) would not permit elution with either NaCl or $MgCl_2$. The abridged affinity had only a modest effect on the pH gradient, with C5 still eluting around pH 2.8.

The E141A/ H164A double mutant (k_{off} =4.0E-03s^{-1}) was the next mutant trialled as an affinity purification reagent. With this mutant, C5 was captured and then eluted with either 2M NaCl or 3M $MgCl_2$. C5 did not respond favourably to elution with high NaCl, irreversibly precipitating when eluted at 2M and eluting at 1M in a broad, flat peak. Conversely, 3M $MgCl_2$ gave a sharp, symmetrical elution peak with no visible precipitation in the fractions. We tested lower concentrations of $MgCl_2$ and found we could elute C5 using a 2M solution, but with a 1M solution tailing of the peak was observed.

After a gel filtration step we tested the purified C5 to ascertain its quality and functional activity (Figure 4). The final material was pure by SDS PAGE, the thermal melt was consistent with commercially available C5 by DSC, and it bound to wt OmCI with high affinity, <100 pM, in a multi-cycle kinetics experiment. Crucially, the material was functionally active and restored activity to C5-depleted serum in an AP activation ELISA, with a pEC50 of 7.1 -log M.

The E141A/R47A double mutant (k_{off} =3.2E-02 s^{-1}) proved to have too fast a dissociation rate to retain C5 on the column prior to elution.

Discussion

In silico and biophysical analysis of the C5-OmCI interaction has identified residues that contribute significantly to the high binding affinity. We show that the OmCI-C5 interaction is complex and higher affinity than previously thought, and we demonstrate the utility of affinity attenuated OmCI as a purification reagent.

The *in silico* mutagenesis, performed using MOE, identified seven residues which could significantly alter binding energy, including five charged residues that potentially contribute to the formation of either salt bridges or hydrogen bonds.

The C5-OmCI-RaCI crystal structure suggests there are two ionic interactions between C5 and OmCI, arising from a bidentate salt bridge between $E141_{OmCI}$ and $R1226_{C5}$. Experimentally, E141A was the most effective single mutation, which highlights the importance of the salt bridge interactions.

The other polar residues lack suitably charged opposing residues on C5 with which to make ionic interactions, and instead make inter-chain hydrogen bonds. In the structure, $H164_{OmCI}$ and $H117_{OmCI}$ appear to make hydrogen bonds with the backbone carbonyl groups of $P1221_{C5}$ and $S1236_{C5}$, respectively. Two residues appear to make bidentate hydrogen bonds: $D167_{OmCI}$ with the backbone

amide groups of $R955_{C5}$ and $R956_{C5}$; and $R47_{OmCI}$ with the side chain carbonyl and amide groups of $N1221_{C5}$.

Experimentally, the rank order of affinity of the hydrogen bonding residues was broadly as per the predictions in MOE, with the K_D of H164A < D167A< H117A. However, our analysis in MOE overestimated the impact of the H164A mutation relative to removal of the E141 salt bridge and underestimated the importance of the R47A mutation. The H164A mutation was predicted to be the most attenuating single mutation but it was found to be less effective than either E141A or R47A.

Two hydrophobic residues, $M134_{OmCI}$ and $L140_{OmCI}$, were also identified in the MOE analysis. Both are adjacent to charged residues ($D135_{OmCI}$ and $E141_{OmCI}$ respectively), and may have been identified as either lowering the desolvation or conformational entropy of their polar neighbours. We had predicted that L140G would be the third most effective mutation, but as a single mutation it was largely ineffective and made only a modest contribution when used in combination.

The single M134G mutation virtually attenuated binding, but CD and DSC data, suggest this is likely to be due to instability arising from a loss of secondary structure. M134 is at the end of a β-sheet and the insertion of a flexible glycine residue may be poorly tolerated in this position.

M134 marks the end of BH-α3, a predominantly hydrophobic loop on which L140G is situated, connecting the large α3 helix of OmCI to the β-barrel fold. In complex with C5, this loop nestles in a hydrophobic channel on the C5d domain, bordered by $A1216_{C5}$-$V1218_{C5}$ and $S123_{C5}$-$V1239_{C5}$. Although the region is hydrophobic, inter chain hydrogen bonds appear to form between the backbone moieties. These are not side chain interactions and subsequently could not be easily investigated by mutagenesis, but they may still contribute significantly to the free energy of binding, with the hydrophobic environment ensuring a low desolvation entropy.

Finally, the control mutation, $F36W_{OmCI}$, showed only a slight increase in k_{off} value, as expected. While this mutant still displayed high affinity binding to C5, this may indicate a subtle allosteric effect arising from this distal mutation.

Overall the structure-based *in silico* approach was effective in designing mutations, reducing the number of mutants that had to be made and tested. While there were some notable outliers in the ranking there is a reasonable correlation with our experimental data.

When considering binding modes, our single-cycle kinetics experiments suggested the potential for a complex interaction, that while displaying refractive index changes consistent with a 1:1 stoichiometry, was not best described with a one site binding model. We performed multi-cycle kinetics, with site specific immobilisation of OmCI via an N-terminal tag, and observed similar outcomes when fitting data using the single site binding model, suggesting that the complex kinetics are not the result of a heterogenous immobilisation. Both the C5d and CUB domains interact with OmCI and this creates the potential for multiple binding modes should an interaction with either domain be made first.

C5 displays a biphasic unfolding when thermally denatured. A main peak unfolds at 60 ºC, with a shoulder at 69°C, and a second smaller unfolding occurs at 77 ºC. The shoulder of the main peak observed in C5 may be of interest, as it closely matches the Tm of the main peak in the C5-wt OmCI complex. This may suggest that OmCI is selecting a naturally occurring C5 conformation in which C5 is resistant to cleavage by the C5 convertases.

The smaller unfolding at 77 ºC may also arise from a conformer of C5. If this is the case, the small size of the peak, corresponding to the enthalpy of unfolding, would suggest that the conformation is infrequently sampled. While OmCI may bind to and stabilise the conformer, increasing Tm, the ΔH remains broadly consistent which suggests it is not a conformation that OmCI selects for or induces.

Alternatively, this could be a more stable domain that is structurally distinct from the MG domains which constitute a large proportion of C5, potentially either the C5d, CUB or C345C domains. Complexing with OmCI appears to stabilise this domain by +3 ºC but there is not a clear correlation to affinity when complexed with mutant OmCI. The lack of correlation to affinity could indicate an interaction between C5-OmCI that is not within the binding interface, as seen in the crystal structure, and

therefore is not attenuated by our mutations provided full occupancy is maintained.

When looking at the charge profile of the surface of C5 and OmCI we noted a positively charged cavity between the C5d and CUB domains (Figure S4). The surface of OmCI is negatively charged and there may be further complementary charge interactions with this cavity that are prevented by $F1631_{C5}$ protruding from the C345C domain and occluding the cavity (Figure 1A). The position and proximity of the flexible C345C domain appears to be the result of crystal contacts between C5 molecules, rather than a specific interaction with the OmCI protein, suggesting that this positively charged region on C5 may be accessible in solution.

When testing our mutants in AP ELISA, we did not see reductions in Emax as a result of removing contacts which would have indicated allosteric inhibition. Our mutants behave in the functionally competitive manner of the wt, which could indicate a competitive or steric mechanism for OmCI inhibition.

Our affinity attenuated forms of OmCI are useful tools for the purification of C5; they are highly expressed and able to refold after complete denaturation at 100°C. It is fortunate that the mutations decreased k_{off} specifically, with only modest effects on k_{on}, and as such are ideal capture reagents for affinity columns. Our final purification reagent, E141A, H164A OmCI, is thermally stable and resilient to denaturation. The elution conditions this mutant has enabled are comparatively gentle, with no evidence of C5 activation with short term exposure to 2M $MgCl_2$. This reagent will be a valuable tool for the purification of C5 to support research and drug discovery.

Experimental Procedures

Design of mutations

Molecular Operating Environment (MOE 2016.08) was used to virtually mutate individual OmCI residues to alanine in the crystal co-complex structure of OmCI-C5 (PDB code: 5HCC). The effect of these changes on the C5 interaction were scored using a binding free energy prediction (dAffinity). Alanine and glycine mutations that lowered dAffinity by more than 1 Kcal/mol were selected for experimental validation.

Construct design

A DNA sequence, comprising the wt OmCI reference sequence (Uniprot entry: Q5YD59), with a n-terminal AVI-tag peptide sequence (GLNDIFEAQKIEWHE) and poly-Histidine tag, was designed using Vector NTI. In total 15 gene variants were designed with single or double mutations to validate the *in silico* affinity predictions. The amino acid sequence of the OmCI proteins can be found in Figure S5. Custom synthesis and cloning into a mammalian expression vector was performed by ATUM.

Small scale expression and purification

Plasmid DNA for each construct was amplified using QIAGEN Plasmid Plus Giga Kits and quantified by A260. Individual 50ml ExpiHEK 293 cell cultures, at 3x106 cells/mL, per construct, were set up using Expifectamine 293 Transfection kits (Invitrogen), as per the manufacturer's instructions. The cells were cultured for four days and centrifuged at 4000 rpm for one hour.

The supernatants were filtered through a 0.22 µm sterifilter and each sample purified on 1.0 mL of Ni Sepharose® Excel capture resin (GE Healthcare). The following modifications were made to the manufacturer's protocol: after binding, affinity captured protein was washed with 20x resin volume using Buffer A (0.5 M NaCl, 0.02 M Imidazole, PBS pH 7.3). Protein samples were then eluted using Buffer B (0.5 M NaCl, 0.25 M Imidazole, PBS (pH7.3) as 10x 2 mL fractions. Post elution, the proteins were concentrated and buffer exchanged using 10 kDa spin concentrators (MerckMillipore). The protein concentration was determined by A280 and the samples were analysed by SDS PAGE before storage at -80 °C.

Bir-A biotinylation of AVI tagged OmCI

Biotinylation of the n-terminal AVI tag was performed using a Bir-A labelling kit (Avidity), as per manufacturer's instructions. OmCI protein was buffer exchanged in 10mM Tris, pH 8.0, using 2mL Zeba desalting columns (Thermo Fisher) and diluted to 40 µM. Bir-A enzyme was added at 11.625 ug/mL and BioMix B was added at 10% (v/v). An overnight incubation at RT was performed. Prior to use, unreacted biotin was removed using a PD-10 desalting column (GE Healthcare).

Surface Plasmon Resonance – single-cycle kinetics

Experiments were performed using a Biacore 8K (GE Healthcare). The OmCI mutants were immobilised on a CM5 chip using amine coupling. To achieve a minimal immobilisation both flow cells were activated using EDC/NHS at a 1:2 molar ratio (flow rate 10 µL/min, contact time 30 s). Solutions of OmCI at 1 ug/mL were prepared in pH 4.5 Sodium acetate buffer and immobilised on flow cell two only (flow rate 10 µL/min, contact time 420 s). Finally, ethanolamine was applied to both flow cells (flow rate 10 µL/min, contact time 420 s). A final immobilisation level of *ca* 50 RU was obtained.

Single-cycle kinetics were measured using a nine point, three-fold titration of C5 (CompTech) from 500nM in HBS-EP buffer. A high flow rate of 40 µL/min was used, with a contact time of 230 s and a dissociation time of 900 s. Binding to the reference surface was subtracted and data fitted to a single site binding model, using Biacore Evaluation Software.

Differential Scanning Calorimetry

DSC was performed using a Malvern Microcal VP Capillary DSC. Samples of C5 (CompTech) and OmCI protein were diluted to 1 mg/mL in PBS. For complexing experiments, C5 and OmCI were mixed in 1:1.25 molar ratio and incubated for a minimum of six hours at 4 ºC. Samples were heated from 10ºC to 100ºC at a rate of 1ºC/min. The injection speed was 50uL/s with three filling strokes used. Six buffer reads were measured prior to running samples and a clean, consisting of three cycles of 20 minute detergent incubations at 80 ºC, was performed after each sample. For refolding experiments, after cooling for 1 hour, a single rescan was performed under the same analysis parameters. Data were analysed using Origin 7.0 software and fitted using a non-two state, cursor initiated model.

Circular Dichroism

OmCI protein was buffer exchanged into 20 mM phosphate, pH 7.4, 150 mM NaF using 0.5 mL Zeba desalting columns (Thermo Fisher). CD spectra were acquired using a scan range of 185-260nm, with a step size of 0.5nm, a time-per-point of 1s and a bandwidth of 1nm. The concentration of protein was 0.3mg/mL and the cuvette pathlength was 1.0 mm.

An air blank was measured and automatically subtracted and a buffer blank was measured and manually subtracted from the spectra.

Surface Plasmon Resonance- multi-cycle kinetics

Multi cycle kinetics were measured using a Biacore 8K (GE Healthcare). Site specifically biotinylated OmCI protein was diluted to 5 nM in HBS-EP. Both flow cells of an SA strepatvidin chip were prepared by performing three sequential injections of 1M NaCl, 20mM NaOH (flow rate 10 µL/min, contact time 60 s). OmCI was then injected over flow cell 1 (flow rate 10 µL/min, contact time 60 s). Final immobilisation levels in the range of 20-100 RU were obtained. A wash of the fluidics with a 1:1 mixture of isopropanol and 1M NaCl, 20mM NaOH was performed, prior to running samples.

A seven point, three-fold titration of C5 (CompTech) was prepared in HBS-EP buffer from 250nM. This was injected at a flow rate of 30 µL/min, with a contact time of 240 s and a dissociation time of 3600 s. After each injection, the surface was regenerated with two sequential injections of 0.1M citric acid monohydrate (pH 2.0) with a contact time of 30 s and flow rate of 30 µL/min.

Binding to the reference surface was subtracted and data fitted to a single site binding model, using Biacore Evaluation Software. When fitting data, curves at concentrations >18.5nM (20-200x [K_D]) were excluded from the analysis to maximise curvature and increase the accuracy of fitting K_{on}.

Complement Activation ELISA

An Alternative Pathway Complement ELISA (Wieslab) was run as per the manufacturer's instructions. Ten point, three-fold titrations of OmCI were made from 5 µM in human serum (TCS Bioscience) and allowed to incubate for 30 minutes at RT, prior to receiving a 1/18 dilution into assay diluent. The diluted samples were immediately plated onto the assay plate.

For experiments with purified C5, C5 was titrated from 5 µM in C5 depleted serum

(Comptech), immediately diluted 1/18 into assay diluent and plated.

Data was analysed using a 4-parameter logistic fit in Prism 7.02.

Ammonium sulphate precipitation

Human serum (TCS Bioscience) was thawed in a 37ºC water bath. The serum was cooled to 4ºC and 60mL of a saturated ammonium sulphate solution was added dropwise per 100mL of serum, with gentle stirring. The precipitate was collected by centrifugation at 10,000 xg for 30 minutes at 4 ºC. The pellet was resuspended to the original serum volume using PBS, 10mM EDTA and a second round of precipitation performed. Prior to loading on the column, the sample was filtered through a 0.22 µM sterifilter.

Purification of C5 using affinity attenuated OmCI

Using an Akta pure (GE Healthcare), biotinylated E141A, H164A OmCI was diluted to 20 µM and 2.0mL was injected onto a 1mL Hi-Trap Streptavidin HP column (GE Healthcare) at a flow rate of 0.5mL/min.

The column was equilibrated with 5x column volumes (CV) of PBS. Ammonium sulphate precipitated serum was loaded at a flow rate of 0.5 mL/min and a 5x CV wash with PBS at a flow rate of 1mL/min was performed. C5 was eluted and collected in fractions, using an isocratic elution of 5x CV 20mM Tris, 2M $MgCl_2$, at a flow rate of 1mL/min.

Immediately after elution, the fractions were pooled and injected onto a HiLoad 16/600 Superdex 200 pg gel filtration column (GE Healthcare), that had been pre-equilibrated with PBS. The column was run at 1mL/min and all peaks were collected. The peaks were analysed by SDS PAGE and those with a molecular weight consistent with C5 monomer were pooled and stored at -80 ºC.

Acknowledgements:

We would like to thank Professor Susan Lea for highlighting the utility of OmCI as a purification tool and Dr John Sinfield from GE Healthcare for helpful discussions on our Biacore data.

Conflicts of interest:

The work has been funded by UCB. Except for J.v.d.E, all authors are UCB employees and may hold shares and/or share options in UCB.

References

1. Rawal, N., and Pangburn, M. K. (1998) C5 convertase of the alternative pathway of complement. Kinetic analysis of the free and surface-bound forms of the enzyme. *J Biol Chem* **273**, 16828-16835
2. Pangburn, M. K., and Rawal, N. (2002) Structure and function of complement C5 convertase enzymes. *Biochem Soc Trans* **30**, 1006-1010
3. Woodruff, T. M., Nandakumar, K. S., and Tedesco, F. (2011) Inhibiting the C5-C5a receptor axis. *Mol Immunol* **48**, 1631-1642
4. Gerard, N. P., and Gerard, C. (1991) The chemotactic receptor for human C5a anaphylatoxin. *Nature* **349**, 614-617
5. DiScipio, R. G., Linton, S. M., and Rushmere, N. K. (1999) Function of the factor I modules (FIMS) of human complement component C6. *J Biol Chem* **274**, 31811-31818
6. Hadders, M. A., Bubeck, D., Roversi, P., Hakobyan, S., Forneris, F., Morgan, B. P., Pangburn, M. K., Llorca, O., Lea, S. M., and Gros, P. (2012) Assembly and regulation of the membrane attack complex based on structures of C5b6 and sC5b9. *Cell Rep* **1**, 200-207
7. Serna, M., Giles, J. L., Morgan, B. P., and Bubeck, D. (2016) Structural basis of complement membrane attack complex formation. *Nat Commun* **7**, 10587
8. Aleshin, A. E., DiScipio, R. G., Stec, B., and Liddington, R. C. (2012) Crystal structure of C5b-6 suggests structural basis for priming assembly of the membrane attack complex. *J Biol Chem* **287**, 19642-19652
9. Jore, M. M., Johnson, S., Sheppard, D., Barber, N. M., Li, Y. I., Nunn, M. A., Elmlund, H., and Lea, S. M. (2016) Structural basis for therapeutic inhibition of complement C5. *Nat Struct Mol Biol* **23**, 378-386

10. Schatz-Jakobsen, J. A., Zhang, Y., Johnson, K., Neill, A., Sheridan, D., and Andersen, G. R. (2016) Structural Basis for Eculizumab-Mediated Inhibition of the Complement Terminal Pathway. *J Immunol* **197**, 337-344
11. Rawal, N., and Pangburn, M. K. (2001) Structure/function of C5 convertases of complement. *Int Immunopharmacol* **1**, 415-422
12. Rawal, N., and Pangburn, M. K. (2003) Formation of high affinity C5 convertase of the classical pathway of complement. *J Biol Chem* **278**, 38476-38483
13. Hill, A. (2005) Eculizumab for the treatment of paroxysmal nocturnal hemoglobinuria. *Clin Adv Hematol Oncol* **3**, 849-850
14. Hillmen, P., Muus, P., Roth, A., Elebute, M. O., Risitano, A. M., Schrezenmeier, H., Szer, J., Browne, P., Maciejewski, J. P., Schubert, J., Urbano-Ispizua, A., de Castro, C., Socie, G., and Brodsky, R. A. (2013) Long-term safety and efficacy of sustained eculizumab treatment in patients with paroxysmal nocturnal haemoglobinuria. *Br J Haematol* **162**, 62-73
15. Licht, C., Greenbaum, L. A., Muus, P., Babu, S., Bedrosian, C. L., Cohen, D. J., Delmas, Y., Douglas, K., Furman, R. R., Gaber, O. A., Goodship, T., Herthelius, M., Hourmant, M., Legendre, C. M., Remuzzi, G., Sheerin, N., Trivelli, A., and Loirat, C. (2015) Efficacy and safety of eculizumab in atypical hemolytic uremic syndrome from 2-year extensions of phase 2 studies. *Kidney Int* **87**, 1061-1073
16. Rathbone, J., Kaltenthaler, E., Richards, A., Tappenden, P., Bessey, A., and Cantrell, A. (2013) A systematic review of eculizumab for atypical haemolytic uraemic syndrome (aHUS). *BMJ Open* **3**, e003573
17. Lockington, D., Imrie, F., Gillen, J., Fitzpatrick, A., and Willison, H. (2010) Visual improvement in established central retinal vein occlusion with long-standing macular edema following systemic eculizumab treatment. *Can J Ophthalmol* **45**, 649
18. Yehoshua, Z., de Amorim Garcia Filho, C. A., Nunes, R. P., Gregori, G., Penha, F. M., Moshfeghi, A. A., Zhang, K., Sadda, S., Feuer, W., and Rosenfeld, P. J. (2014) Systemic complement inhibition with eculizumab for geographic atrophy in age-related macular degeneration: the COMPLETE study. *Ophthalmology* **121**, 693-701
19. Howard, J. F., Jr., Barohn, R. J., Cutter, G. R., Freimer, M., Juel, V. C., Mozaffar, T., Mellion, M. L., Benatar, M. G., Farrugia, M. E., Wang, J. J., Malhotra, S. S., Kissel, J. T., and Group, M. G. S. (2013) A randomized, double-blind, placebo-controlled phase II study of eculizumab in patients with refractory generalized myasthenia gravis. *Muscle Nerve* **48**, 76-84
20. Howard, J. F., Jr., Utsugisawa, K., Benatar, M., Murai, H., Barohn, R. J., Illa, I., Jacob, S., Vissing, J., Burns, T. M., Kissel, J. T., Muppidi, S., Nowak, R. J., O'Brien, F., Wang, J. J., Mantegazza, R., and Group, R. S. (2017) Safety and efficacy of eculizumab in anti-acetylcholine receptor antibody-positive refractory generalised myasthenia gravis (REGAIN): a phase 3, randomised, double-blind, placebo-controlled, multicentre study. *Lancet Neurol* **16**, 976-986
21. Pittock, S. J., Lennon, V. A., McKeon, A., Mandrekar, J., Weinshenker, B. G., Lucchinetti, C. F., O'Toole, O., and Wingerchuk, D. M. (2013) Eculizumab in AQP4-IgG-positive relapsing neuromyelitis optica spectrum disorders: an open-label pilot study. *Lancet Neurol* **12**, 554-562
22. Johnson, C. K., and Leca, N. (2015) Eculizumab use in kidney transplantation. *Curr Opin Organ Transplant* **20**, 643-651
23. Kaabak, M., Babenko, N., Shapiro, R., Zokoyev, A., Dymova, O., and Kim, E. (2018) A prospective randomized, controlled trial of eculizumab to prevent ischemia-reperfusion injury in pediatric kidney transplantation. *Pediatr Transplant* **22**
24. Morgan, B. P., and Harris, C. L. (2015) Complement, a target for therapy in inflammatory and degenerative diseases. *Nat Rev Drug Discov* **14**, 857-877
25. Ricklin, D., and Lambris, J. D. (2016) New milestones ahead in complement-targeted therapy. *Semin Immunol* **28**, 208-222
26. Fredslund, F., Laursen, N. S., Roversi, P., Jenner, L., Oliveira, C. L., Pedersen, J. S., Nunn, M. A., Lea, S. M., Discipio, R., Sottrup-Jensen, L., and Andersen, G. R. (2008) Structure of and influence of a tick complement inhibitor on human complement component 5. *Nat Immunol* **9**, 753-760

27. Roversi, P., Lissina, O., Johnson, S., Ahmat, N., Paesen, G. C., Ploss, K., Boland, W., Nunn, M. A., and Lea, S. M. (2007) The structure of OMCI, a novel lipocalin inhibitor of the complement system. *J Mol Biol* **369**, 784-793
28. Roversi, P., Ryffel, B., Togbe, D., Maillet, I., Teixeira, M., Ahmat, N., Paesen, G. C., Lissina, O., Boland, W., Ploss, K., Caesar, J. J., Leonhartsberger, S., Lea, S. M., and Nunn, M. A. (2013) Bifunctional lipocalin ameliorates murine immune complex-induced acute lung injury. *J Biol Chem* **288**, 18789-18802
29. Hepburn, N. J., Williams, A. S., Nunn, M. A., Chamberlain-Banoub, J. C., Hamer, J., Morgan, B. P., and Harris, C. L. (2007) In vivo characterization and therapeutic efficacy of a C5-specific inhibitor from the soft tick Ornithodoros moubata. *J Biol Chem* **282**, 8292-8299
30. Laursen, N. S., Andersen, K. R., Braren, I., Spillner, E., Sottrup-Jensen, L., and Andersen, G. R. (2011) Substrate recognition by complement convertases revealed in the C5-cobra venom factor complex. *EMBO J* **30**, 606-616
31. Flower, D. R., North, A. C., and Sansom, C. E. (2000) The lipocalin protein family: structural and sequence overview. *Biochim Biophys Acta* **1482**, 9-24
32. Kuhn, N., Schmidt, C. Q., Schlapschy, M., and Skerra, A. (2016) PASylated Coversin, a C5-Specific Complement Inhibitor with Extended Pharmacokinetics, Shows Enhanced Anti-Hemolytic Activity in Vitro. *Bioconjug Chem* **27**, 2359-2371
33. Nishimura, J., Yamamoto, M., Hayashi, S., Ohyashiki, K., Ando, K., Brodsky, A. L., Noji, H., Kitamura, K., Eto, T., Takahashi, T., Masuko, M., Matsumoto, T., Wano, Y., Shichishima, T., Shibayama, H., Hase, M., Li, L., Johnson, K., Lazarowski, A., Tamburini, P., Inazawa, J., Kinoshita, T., and Kanakura, Y. (2014) Genetic variants in C5 and poor response to eculizumab. *N Engl J Med* **370**, 632-639
34. Volk, A. L., Hu, F. J., Berglund, M. M., Nordling, E., Stromberg, P., Uhlen, M., and Rockberg, J. (2016) Stratification of responders towards eculizumab using a structural epitope mapping strategy. *Sci Rep* **6**, 31365
35. Sjoholm, A. G. (1975) Complement components in normal serum and plasma quantitated by electroimmunoassay. *Scand J Immunol* **4**, 25-30
36. Sottrup-Jensen, L., and Andersen, G. R. (2014) Purification of human complement protein C5. *Methods Mol Biol* **1100**, 93-102
37. Dessauer, A., and Rother, U. (1983) The fifth component of complement (C5): purification without activation. *Immunobiology* **164**, 370-379
38. Wetsel, R. A., Jones, M. A., and Kolb, W. P. (1980) Immunoadsorbent affinity purification of the fifth component (C5) of human complement and development of a highly sensitive hemolytic assay. *J Immunol Methods* **35**, 319-335
39. Kunkel, S. L., Kreutzer, D. L., Goralnick, S., and Ward, P. A. (1980) Purification of the third and fifth components of human complement: application of hydrophobic chromatography. *J Immunol Methods* **35**, 337-351
40. (2018) Molecular Operating Environment (MOE). 2013.08 Ed., Chemical Computing Group ULC, 1010 Sherbooke St. West, Suite #910, Montreal, QC, Canada, H3A 2R7
41. Luck, U. R. a. L. A. (2007) Molecular Modeling of Estrogen Receptor Using Molecular Operating Environment. *Biochemistry and Molecular Biology Education* **35**, 238-243
42. Nunn, M. A., Lea, S. M., and Roversi, P. C. (2016) Modified omci as a complement inhibitor. Google Patents
43. Onell, A., and Andersson, K. (2005) Kinetic determinations of molecular interactions using Biacore--minimum data requirements for efficient experimental design. *J Mol Recognit* **18**, 307-317

Table 1
Summary table of key data generated with OmCI proteins, showing the selection of a small panel of mutants for profiling as a purification ligand.

	***In silico* prediction**	**Single-cycle kinetics [1]**	**CD**	**DSC[2]**		**AP ELISA**	**Multi-cycle kinetics**		
OmCI Mutation	**dAffinity score (kcal/ mol)**	**Approximate fold change in k_{off}**	**Loss of secondary structure (217 nm)**	**ΔTm (°C)**	**ΔΔH (% refolded)**	**pIC50 (-log M)**	**k_{on} (1/Ms)**	**k_{off} (1/s)**	**K_D (M)**
Wild type OmCI	-	-	N	-	71.7	≤ 9.0	5.88E+05	<1.0E-05	<1.0E-10
F36W	0	2.6							
D167A	1.9	2.4							
H117A	2.3	1.1							
R47A	3.1	4.1	N	-4.8	69.1	≤ 9.0			
M134G	4.3	229.0	Y	-8.2	23.9				
L140G	5.4	1.0							
E141A	5.8	29.1	N	-3.3	61.7	≤ 8.9	4.81E+05	3.04E-04	7.09E-10
H164A	7.6	3.5	N	-1.6	57.7	≤ 8.8			
E141A/ R47A	9.3	973.0	N	3.1	54.1	8.0	3.01E+06	3.18E-02	1.31E-08
E141A/ H164A	11.3	197.0	N	-1.8	47.8	8.5	1.13E+06	4.06E-03	4.09E-09
E141A/ L140G	12.8	31.3							
E141A/ R47A/ M134G	14.6	NB[3]							
E141A/ R47A/ L140G	15.4	1270.0							
E141A/ R47A/ H164A/ L140G	20.4	5500.0							

[1] Single cycle kinetics sensorgrams are shown in Figure S1. A nominal fold change relative to wt k_{off} (approximately 1.0E+05 Ms^{-1}) is shown to exemplify changes in stability of OmCI-C5 complex.
[2] ΔTm values are relative to the wt OmCI protein. Data are shown in Table S1 and Figure 2.
[3] NB = no binding detected.

Table 2
DSC data on C5:OmCI complexes. Data from *n=1* experiment.

Sample	Peak 1 Tm (ºC)	Peak 1 ΔH (cal/M)	Peak 2 Tm (ºC)	Peak 2 ΔH (cal/M)
C5	60.31 ± 0.012	8.1E+05	77.06 ± 0.21	1.1E+05
C5:wt OmCI	68.90 ± 0.020	7.1E+05	81.36 ± 0.21	7.8E+04
C5:E141A OmCI	67.99 ± 0.019	9.6E+05	80.83 ± 0.33	8.1E+04
C5:E141A/ R47A OmCI	66.68 ± 0.016	9.1E+05	80.96 ± 0.28	5.6E+04
C5:E141A/ H164A OmCI	65.41 ± 0.011	8.8E+05	80.49 ± 0.27	5.3E+04

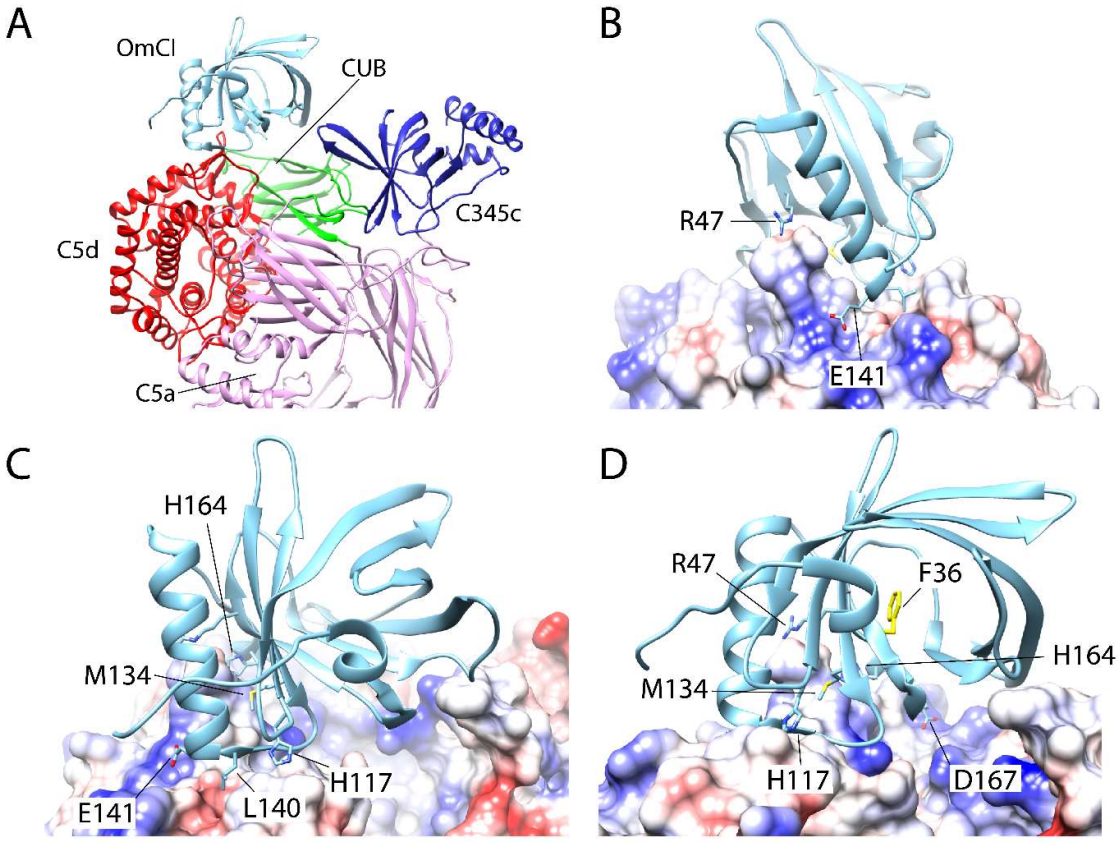

Figure 1. Molecular interactions of the C5-OmCI complex. Panel A shows OmCI in complex with the C5d and CUB domains, on the C5d-CUB-MG8 superdomain of C5 (PDB code: 5HCC). Panel B shows the surface of C5 coloured by charge, with red denoting areas of negative charge and positively charged areas shown in blue. The two OmCI residues that contribute significantly to binding affinity, E141 and R47, are shown. Panel C shows the residues identified from our *in silico* mutagenesis study as contributing significantly to binding affinity, with panel D showing the 180° view.

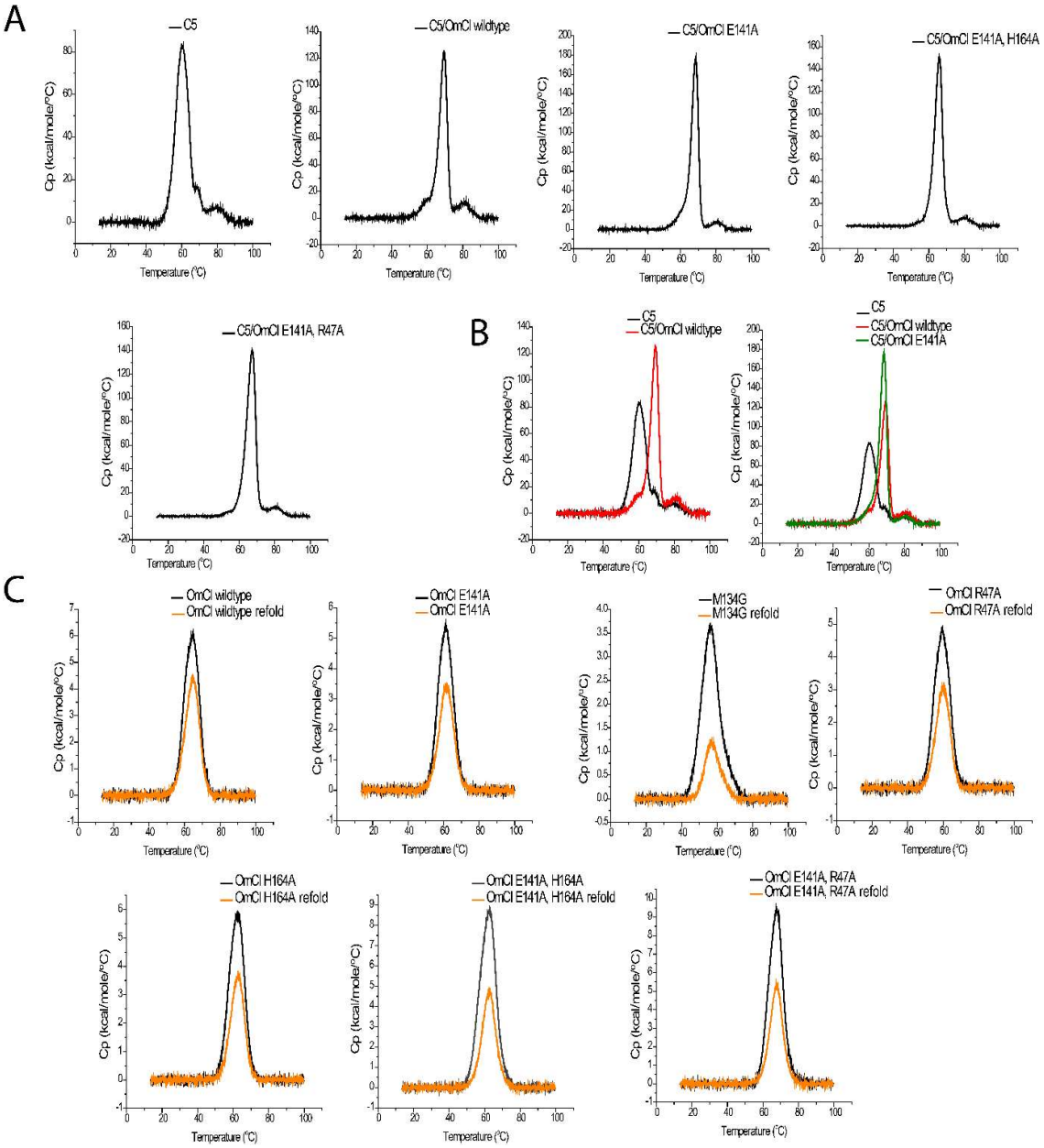

Figure 2. **DSC thermograms for C5 alone and in complex with OmCI proteins.** C5 displays a biphasic unfolding, the main peak has a slight shoulder and unfolds at 60.3 ºC, with a smaller and more stable peak unfolding at 77.1 ºC. Complexing C5 with OmCI stabilises the main peak, in proportion to the binding affinity (panel A). A smaller stabilisation effect, ΔTm = +3 ºC, is observed on the second peak but without clear correlation to the affinity of OmCI construct (Panel B). Panel C shows DSC thermograms for OmCI proteins. The first round of melting is shown in black with the second melt shown in orange. The peak area corresponds to the enthalpy of unfolding (ΔH) and by taking a ratio of the two peaks a ΔΔH or percentage of refolding can be calculated.

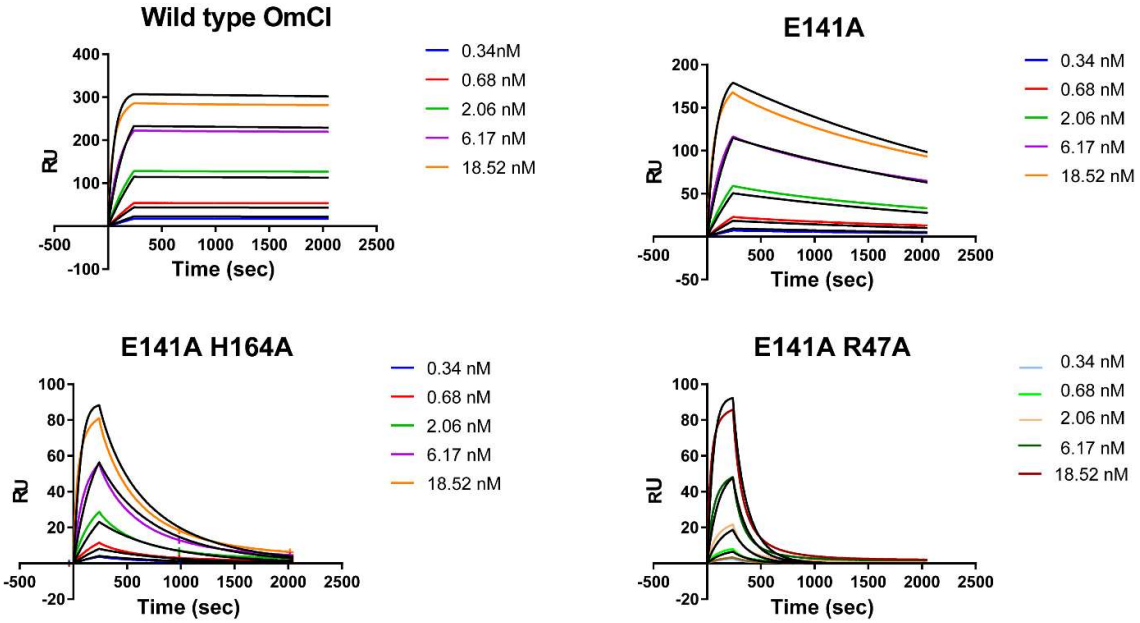

Figure 3. Sensorgrams from multi cycle kinetics. The sensorgrams above show raw data (coloured by concentration) and the fit from a single site binding model (in black). The mutants display an accelerated dissociation relative to wt OmCI. Fitting with the single site model appears to underestimate k_{on} at low concentrations, while at higher concentrations it appears to overestimate it.

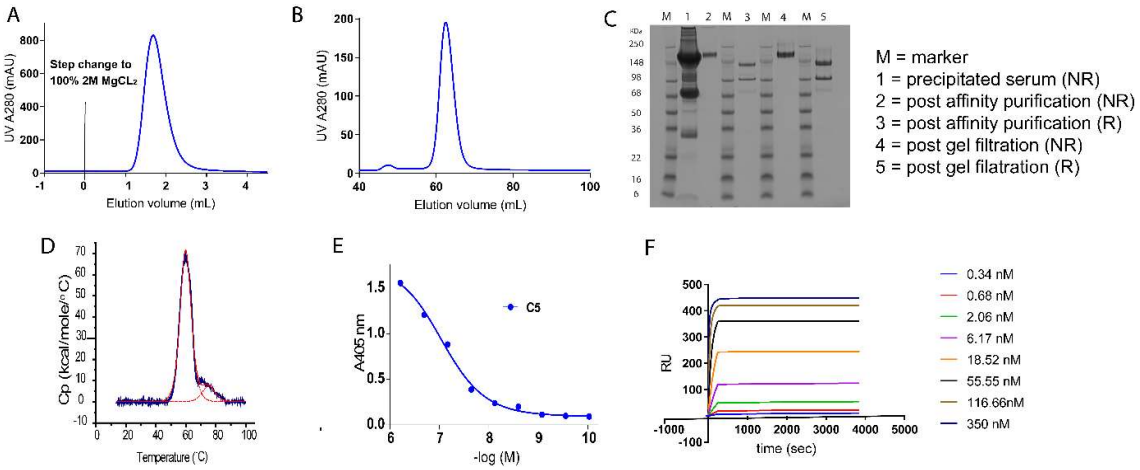

Figure 4. Purification of functional C5 with affinity attenuated E141A/ H164A OmCI mutant. Panel A shows the elution of C5 from an E141A/ H164A OmCI column using isocratic elution with 2M $MgCl_2$, after one column volume the material elutes in a sharp and broadly symmetrical peak. Panel B shows elution of affinity purified C5 from a gel filtration column as a single peak with a small high molecular weight peak. Panel C is a reduced (R) and non-reduced (NR) SDS PAGE gel of the material, pre and post affinity purification and gel filtration (5ug of the final C5 sample is loaded). A thermal melt of the protein by DSC is shown in panel D, with a Tm of 59.9 °C for the main peak. The ability of the material to restore complement activation to C5-depleted serum, with a pEC50 of -7.1 -log M, is shown in panel E. Finally, binding of our purified C5 to wt OmCI is shown in a multi-cycle kinetics experiment, with a K_D <100 pM in Panel F.

The rational design of affinity attenuated OmCI for the purification of Complement C5

Alex Macpherson, Xiaofeng Liu, Neesha Dedi, Jeffery Kennedy, Bruce Carrington, Oliver Durrant, Sam Heywood, Jean van den Elsen and Alastair D. G. Lawson

J. Biol. Chem. published online July 20, 2018

Access the most updated version of this article at doi: 10.1074/jbc.RA118.004043

Supplementary Information

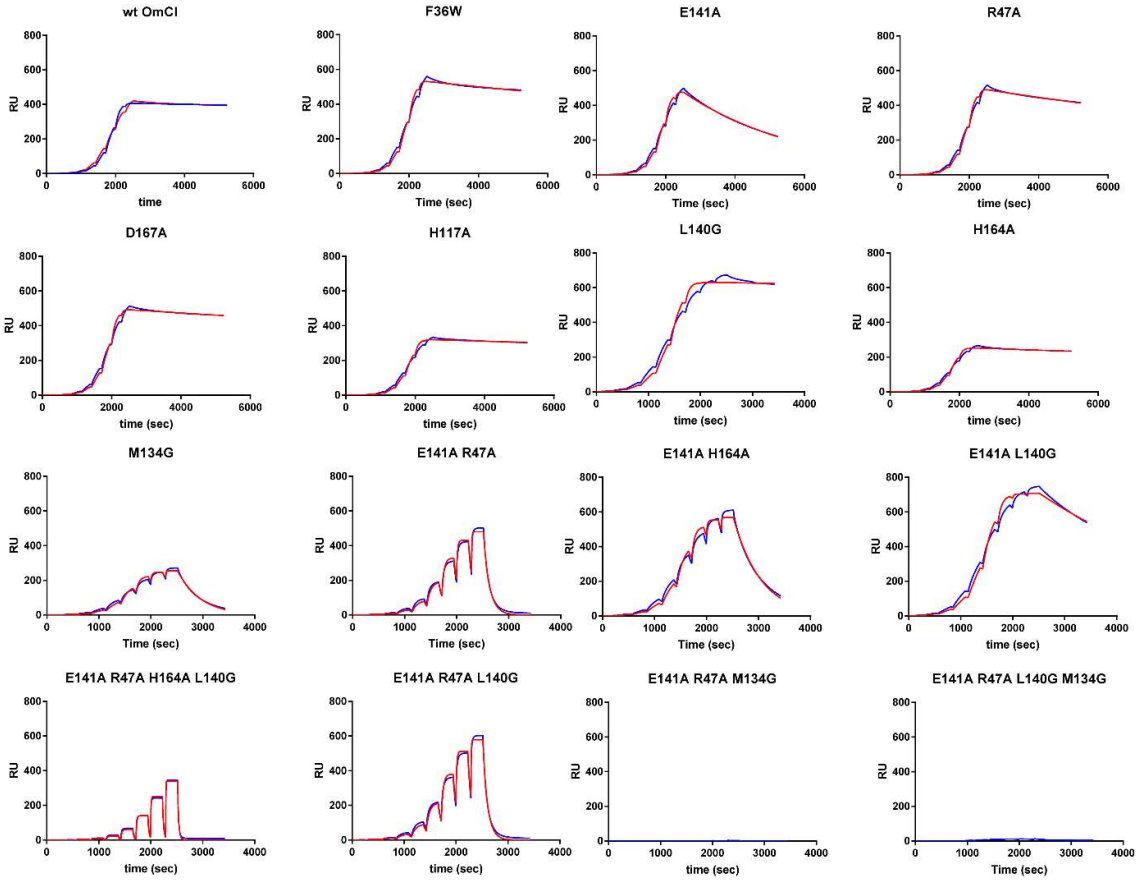

Figure S1. Example Sensorgrams from single cycle kinetics experiments, fitted with a one site binding model. The sensorgrams are shown in blue and the fit in red. The mutants show an accelerated k_{off} during the dissociation phase.

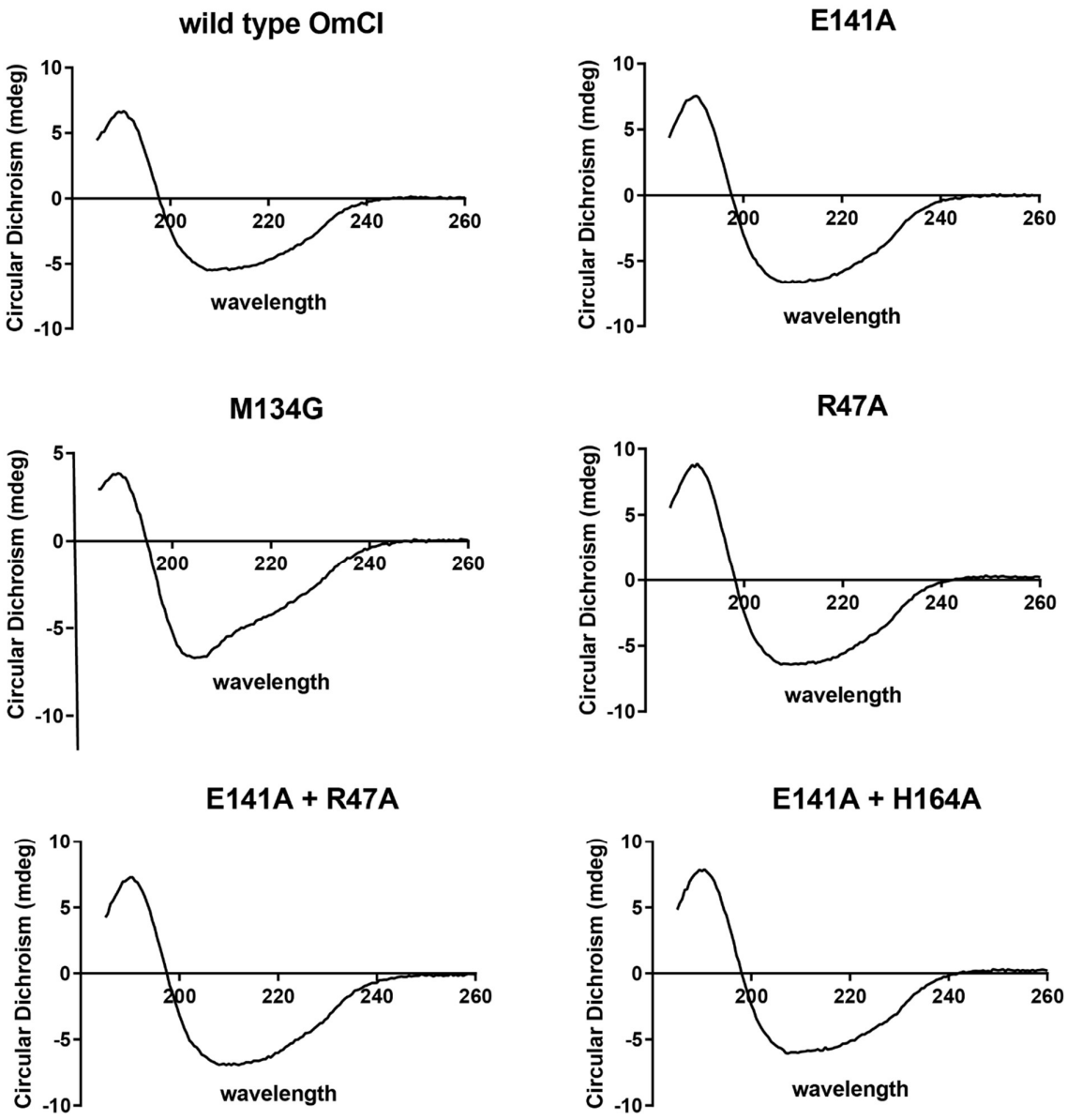

Figure S2. CD traces of OmCI proteins. All mutants show similar profiles by CD apart from M134G, which shows a marked loss of structure at 217nm consistent with a loss of β sheet. A reduction in the positive peak is also observed suggesting a loss of overall secondary structure.

Table S1
DSC data for OmCI proteins. Data from *n=1* experiment.

Mutation	Tm (°C)	ΔTm (°C)	ΔH (Cal/M)	ΔΔH (% refolded)
wt OmCI	64.39 ± 0.015	-	6.2E+04	-
wt OmCI refold	64.47 ± 0.016	+0.1	4.5E+04	71.7
R47A	59.56 ± 0.015	-4.8	4.9E+04	-
R47A refold	59.44 ± 0.012	-5.0	3.4E+04	69.1
E141A	61.08 ± 0.011	-3.3	5.7E+04	-
E141A refold	62.11 ± 0.011	-2.3	3.5E+04	61.7
H164A	62.8 ± 0.013	-1.6	9.2E+04	-
H164A refold	62.63 ± 0.011	-1.8	5.3E+04	57.7
E141A/ R47A	67.46 ± 0.011	+3.1	1.0E+05	-
E141A/ R47A refold	68.02 ± 0.006	+3.6	5.5E+04	54.1
E141A/ H164A	62.64 ± 0.015	-1.8	9.9E+04	-
E141A/ H164A refold	62.61 ± 0.001	-1.8	4.8E+04	47.8
M134G	56.18 ± 0.001	-8.2	4.6E+04	-
M134G refold	56.94 ± 0.001	-7.5	1.1E+04	23.9

Table S2
Multi cycle kinetics data summary table. Data from *n=4* experiments unless stated.

	k_{on} (1/Ms)	**k_{on} 95% CI**	**k_{off} (1/s)**	**k_{off} 95% CI**	**K_D (M)**
wt OmCI	5.88E+05	3.60E+05	<1.0E-05	-	<100pM
E141A	4.81E+05	2.28E+05	3.04E-04	2.20E-05	7.09E-10
E141A R47A	3.01E+06	2.96E+06	3.18E-02	2.57E-02	1.31E-08
E141A H164A*	1.13E+06	4.18E+05	4.06E-03	1.16E-03	4.09E-09

*average from *n=3* experiments

Multicycle kinetics data from individual occasions

n=1

	k_{on} (1/Ms)	K_{on} SE	k_{off} (1/s)	K_{off} SE	KD (M)
OmCI WT	3.84E+05	5.31E+01	<1.0E-05	-	<100pM
OmCI E141A	3.67E+05	9.25E+01	3.07E-04	2.07E-08	8.37E-10
OmCI E141A R47A	9.86E+05	8.49E+02	1.78E-02	5.49E-09	1.80E-08
OmCI E141A H164A	8.55E+05	4.18E+03	4.38E-03	6.37E-08	5.13E-09

n=2

	k_{on} (1/Ms)	K_{on} SE	k_{off} (1/s)	K_{off} SE	KD (M)
OmCI WT	4.00E+05	6.00E+01	<1.0E-05	-	<100pM
OmCI E141A	3.43E+05	3.08E+02	3.07E-04	2.30E-07	8.96E-10
OmCI E141A R47A	1.19E+06	1.33E+03	2.09E-02	2.25E-05	1.76E-08
OmCI E141A H164A	9.13E+05	4.38E+03	4.89E-03	2.41E-05	5.35E-09

n=3

	k_{on} (1/Ms)	K_{on} SE	k_{off} (1/s)	K_{off} SE	KD (M)
OmCI WT	1.14E+06	5.79E+02	<1.0E-05	-	<100pM
OmCI WT E141A	8.30E+05	3.00E+02	3.28E-04	1.68E-07	3.95E-10
OmCI E141A R47A	2.43E+06	2.50E+03	1.76E-02	1.70E-05	7.26E-09
OmCI E141A H164A	1.62E+06	1.66E+03	2.92E-03	2.45E-06	1.80E-09

n=4

	k_{on} (1/Ms)	K_{on} SE	k_{off} (1/s)	K_{off} SE	KD (M)
OmCI WT	4.32E+05	6.36E+01	<1.0E-05	-	<100pM
OmCI E141A	3.86E+05	8.19E+02	2.73E-04	4.04E-07	7.07E-10
OmCI E141A R47A	7.44E+06	3.19E+05	7.11E-02	3.07E-03	9.55E-09
OmCI E141A H164A*	ND	ND	ND	ND	ND

*Curve rejected.

Supplementary Table 3
Alternative pathway activation ELISA. Data from n=3 experiments.

Mutant	$\bar{x}$ pIC50	pIC50 range (n=3)	$\bar{x}$ Hill Slope	$\bar{x}$ Emax (%)
wt OmCI	≤ 9.0	9.0-9.1	>5	99.8
R47A	≤ 9.0	8.9-9.1	3.9	99.1
E141A	≤ 8.9	8.9	2.4	98.7
H164A	≤ 8.8	8.8	2.5	100.2
E141A/ R47A	8.0	8.0-8.1	0.9	94.7
E141A/ H164A	8.5	8.5-8.6	1.3	97.6

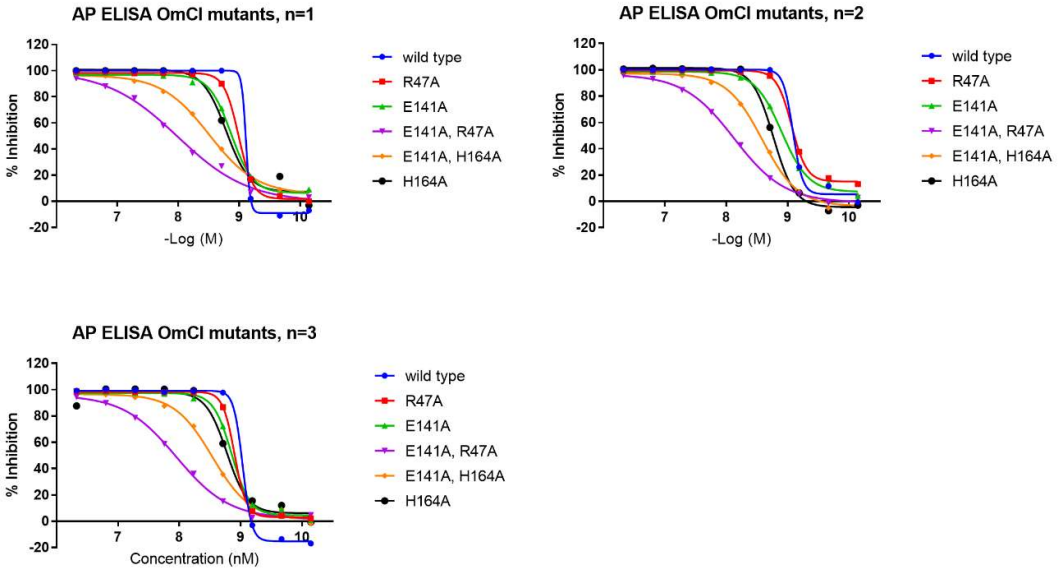

Supplementary Figure 3 Inhibiton of MAC formation in an Alternative Pathway ELISA. The ability of the OmCI mutants to inhibit formation of the MAC was tested by ELISA. The wt protein and single mutants are potent inhibitors and display steep hill slopes. All proteins show full efficacy with Emax values ~100%.

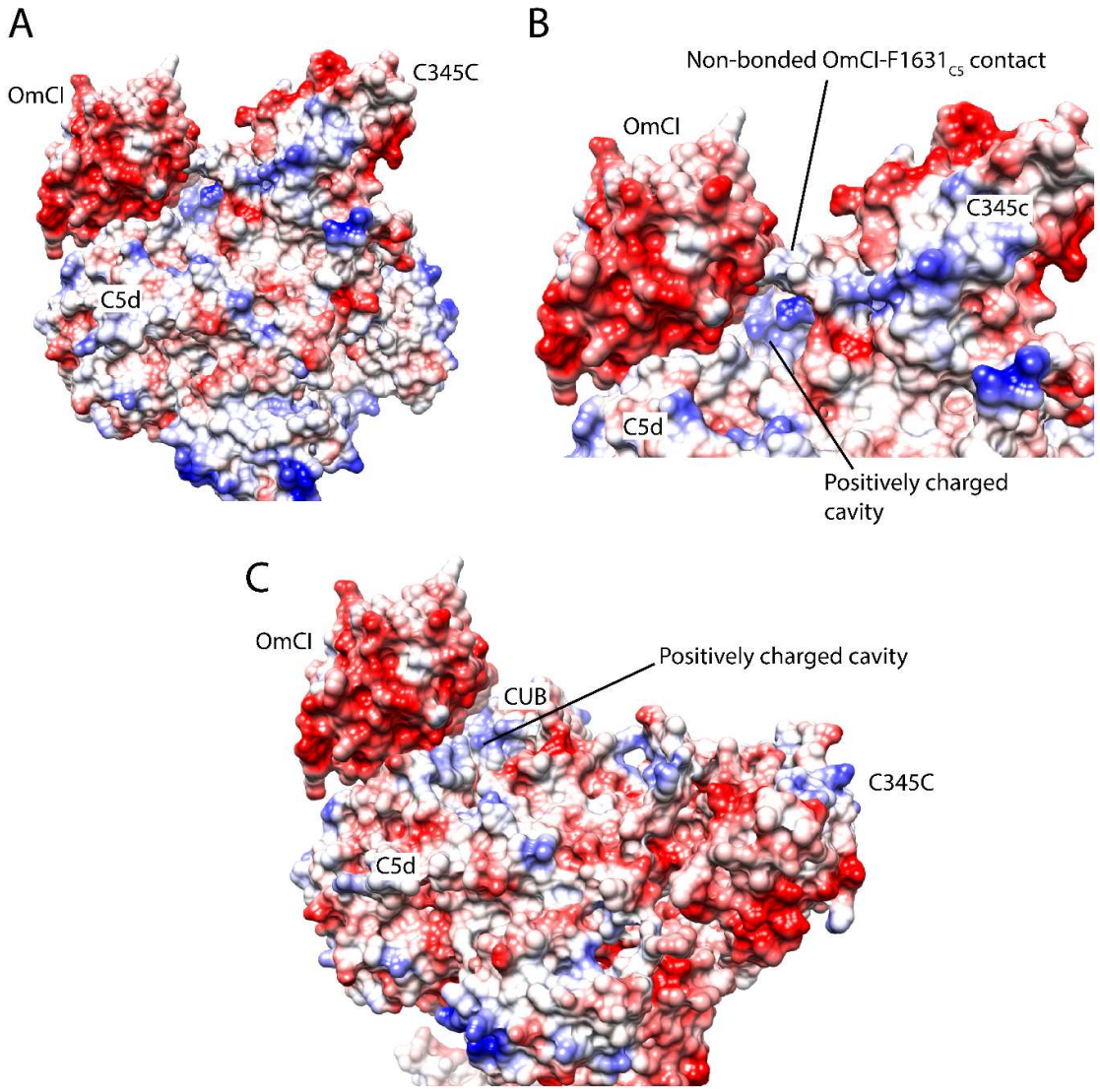

Figure S4. Surface charges of C5 and OmCI. Panel A shows the C5d-CUB-MG8 superdomain of C5 in complex with OmCI (PDB code: 5HCC), the surface is coloured by charge, with blue denoting areas of positive charge and negatively charged areas shown in red. OmCI is predominantly negatively charged. Panel B shows a close-up view of OmCI and C345c showing the non-bonded contact between the two, with a positively charged cavity visible between C5d and CUB domains. Panel C shows the C5d-CUB-MG8 superdomain from the apo C5 structure (PDB code 3CU7) in place of the superdomain from the OmCI-RaCI-C5 structure used in panels A and B. The positively charged cavity is accessible to OmCI when C345C is in the 'down position'.

Amino Acid Sequence for OmCI N-terminal AVI-10xHis

GGSHHHHHHHHHHGSGSENLYFQGSGSASSGLNDIFEAQKIEWHEDSESDCTGSEPVDAFQAFSEGKEA
YVLVRSTDPKARDCLKGEPAGEKQDNTLPVMMTFKNGTDWASTDWTFTLDGAKVTATLGNLTQNREVVY
DSQSHHCHVDKVEKEVPDYEMWMLDAGGLEVEVECCRQKLEELASGRNQMYPHLKDC

Figure S5. Amino acid sequence of OmCI constructs. The amino acid sequence of the final OmCI constructs is shown above. The residues comprising the N-terminal tags are coloured as follows: the 10x Histidine tag in green, a TEV cleavage site in pink and an AVI site in yellow. The residues mutated in the study are coloured cyan.